Atmosphere-Ocean
Publication details, including instructions for authors and subscription information:
http://www.tandfonline.com/loi/tato20

A coupled model simulation of Ocean thermohaline properties of the last glacial maximum

Seong-Joong Kim [a]

[a] Korea Polar Research Institute, KORDI, Ansan P.O. Box 29, Seoul, 425-600, Korea E-mail:

Available online: 21 Nov 2010

To cite this article: Seong-Joong Kim (2004): A coupled model simulation of Ocean thermohaline properties of the last glacial maximum, Atmosphere-Ocean, 42:3, 213-220

To link to this article: http://dx.doi.org/10.3137/ao.420305

A Coupled Model Simulation of Ocean Thermohaline Properties of the Last Glacial Maximum

Seong-Joong Kim*

Korea Polar Research Institute, KORDI
Ansan P.O. Box 29, Seoul 425-600, Korea

[Original manuscript received 5 February 2004; in revised form 19 July 2004]

ABSTRACT *The temperature and salinity of the ocean during the last glacial maximum (LGM) are simulated using a coupled ocean–atmosphere–sea-ice climate model. The imposition of boundary conditions representitive of the LGM leads to deep ocean heat loss to the atmosphere in high latitude convection regions through active vertical mixing and associated turbulent heat fluxes with deepwater temperatures approaching the freezing point. The LGM conditions also modify the freshwater distribution at the ocean surface and cause a marked change in the ocean convection, overturning circulation, and ocean salinity distribution. In the LGM, the ocean becomes substantially fresher in the Atlantic basin due to a freshening of the northern North Atlantic and an associated reduction in North Atlantic Deep Water formation, while the most saline water mass is found in the Southern Ocean as a result of the increase in the formation of sea ice and the drier climate around Antarctica. The LGM thermohaline properties simulated by the coupled model are in reasonable agreement with palaeoclimatic proxy evidence.*

RÉSUMÉ *[traduit par la rédaction] On simule la température et la salinité de l'océan durant le dernier maximum glaciaire à l'aide d'un modèle climatique couplé océan–atmosphère–glaces de mer. L'imposition de conditions aux limites représentatives du dernier maximum glaciaire mène à une perte de chaleur par l'océan profond au profit de l'atmosphère dans les régions de convection des latitudes élevées, sous l'action d'un mélange vertical actif et des flux de chaleur turbulents qui en résultent, ce qui aboutit à des températures de l'eau profonde proches du point de congélation. Les conditions du dernier maximum glaciaire modifient également la distribution de l'eau douce à la surface de l'océan et occasionnent un changement marqué dans la convection océanique, la circulation de renversement des eaux et la distribution de la salinité océanique. Au cours du dernier maximum glaciaire, l'océan devient notablement plus froid dans le bassin atlantique à cause d'un refroidissement de l'Atlantique Nord septentrional et d'une réduction correspondante de la formation d'eau profonde de l'Atlantique Nord, pendant que la masse d'eau la plus saline se retrouve dans la région antarctique en raison de l'augmentation dans la formation de glace de mer et d'un climat plus sec autour de l'Antarctique. Les propriétés thermohalines du dernier maximum glaciaire simulées par le modèle couplé s'accordent raisonnablement avec les preuves paléoclimatiques indirectes.*

1 Introduction

The circulation and properties of the deep ocean play a critical role in regulating the Earth's climate, such as moderating heat and freshwater balances and influencing atmospheric CO_2 concentration (Broecker, 1997). Understanding the glacial/interglacial variations in the deep ocean conditions is, thus, critical in assessing and predicting future climate change.

In the present-day ocean, the deep water is largely comprised of two distinct water masses: relatively warm and saline North Atlantic Deep Water (NADW) and relatively cold and fresh Antarctic Bottom Water (AABW) (Warren, 1981; Killworth, 1983). Formed in the Greenland, Iceland and Norwegian seas and the Labrador Sea (Dickson and Brown, 1994), NADW flows to the Southern Ocean and mixes with the lower part of the Circumpolar Deep Water (LCDW). Flowing eastward as the Antarctic Circumpolar Current, warm, saline, and nutrient poor LCDW spreads northward into the Indian and Pacific oceans. A fraction of LCDW also upwells slowly along the Antarctic continental margin and influences the formation of AABW (Whitworth et al., 1998). AABW is formed in the Weddell Sea, Ross Sea, and along the Adelie Coast (Gill, 1973; Foster and Carmack, 1976; Rintoul, 1998) and mixes with LCDW as it descends to the bottom and spreads northward, filling the abyssal basins of the Atlantic, Indian and Pacific oceans (Orsi et al., 1999). A portion of AABW and LCDW in the Indian–Pacific basins recirculates to the south (Sloyan and Rintoul, 2001) and ventilates at the south of the Antarctic Polar Front, forming the upper part of CDW (UCDW) with oxygen poor and nutrient rich characteristics (Sievers and Nowlin, 1984).

*Author's e-mail: seongjkim@kordi.re.kr

Based on geological and geochemical proxy data, there has been an enormous effort to determine the nature of glacial deepwater mass circulation changes. The preponderance of the proxy evidence suggests that the NADW formation was shallower and formed further south in the North Atlantic during the Last Glacial Maximum (LGM) than at present (Duplessy et al., 1980, 1988; Boyle and Keigwin, 1982, 1987; Curry et al., 1988; Sarnthein et al., 1994; Oppo and Horowitz, 2000; Rutberg et al., 2000, etc.) and in the North Atlantic a large portion of NADW was replaced by water originating in the Southern Ocean with substantially increased nutrient concentrations (Boyle and Keigwin, 1982, 1987). There is some evidence for a continuous glacial-age formation of AABW and enhancement of its outflow toward the Pacific basin (Hall et al., 2001), but the status of the LGM Southern Ocean overturning circulation associated with the AABW production and outflow is still poorly understood.

Knowledge of the LGM deep ocean temperature and salinity from proxy data is becoming available. Earlier estimates suggested that the deep ocean was about 2°C cooler than present day during the LGM (e.g., Broecker and Denton, 1989; Boyle, 1990), but more recent estimates suggest that glacial deep ocean temperatures were within the error range of the freezing point of sea water in all ocean basins (e.g., Boyle, 2002). At present, NADW is more saline than AABW as a result of higher sea surface salinities in the North Atlantic compared to the Antarctic continental margin. In contrast to the present day ocean, the most saline water appears to have been in the Southern Ocean during the LGM (Adkins et al., 2002). These palaeoclimatic proxy estimates imply that during the glacial periods either ocean circulation or surface ocean conditions or both were substantially different from the interglacial periods.

Although geological and geochemical proxy data have provided a broad picture of the LGM deep ocean conditions, these data are limited in their ability to reveal how the deep ocean conditions were determined. As a complement to proxy studies, a hierarchy of physically-based numerical models has been used to study the mechanisms associated with LGM thermohaline circulation and associated properties. One can use simple models to investigate changes in ocean conditions, but these models require the specification of uncertain LGM ocean boundary conditions. Fully coupled models (i.e., models that include three-dimensional representations of atmospheric and oceanic general circulation, including sea-ice physics) are the most comprehensive and physically based tools for simulating the thermohaline circulation and water property changes for the LGM.

Several fully coupled model LGM simulations have been reported (Bush and Philander, 1999; Hewitt et al., 2001; Kitoh et al., 2001; Shin et al., 2003; Kim et al., 2003), but detailed analyses of deepwater properties have not yet been made. The objective of this study is to investigate the response of oceanic thermohaline properties to boundary conditions representative of the LGM using a coupled atmosphere–ocean–sea-ice climate system model.

2 Coupled model and experiments

The model employed in the current study is the second generation Canadian Centre for Climate Modelling and Analysis (CCCma) coupled general circulation model. A detailed description of the atmosphere, ocean, sea ice, and land surface components of the coupled model is given in other papers (Flato and Boer, 2001; Kim et al., 2002, 2003, and references therein) and is briefly summarized here.

The atmospheric component of the coupled model is a primitive equation model characterized by T32 horizontal resolution corresponding to a 3.75° Gaussian grid, and 10 vertical levels (McFarlane et al., 1992). Cloud formation is parametrized through relative humidity and the surface albedo is evaluated depending on the surface type. A simple river routing scheme is included to represent the freshwater flux to the ocean. The oceanic component is a modified version of the Geophysical Fluid Dynamics Laboratory Modular Ocean Model (GFDL MOM) version 1.1 (Pacanowski et al., 1993). The horizontal and vertical resolutions are $1.875° \times 1.875°$ and 29 layers respectively. Ocean mixing is represented by vertical and isopycnal diffusion along with the eddy-induced mixing parametrization of Gent and McWilliams (1990). Isopycnal diffusivity is 1000 $m^2\ s^{-1}$ with a background horizontal diffusivity of 100 $m^2\ s^{-1}$. Vertical diffusivity is 3×10^{-5} $m^2\ s^{-1}$. When the density stratification is unstable, convective adjustment is performed by increasing the vertical diffusivity.

The coupled model includes a representation of sea-ice thermodynamics from Semtner (1976) and sea-ice dynamics from Flato and Hibler (1992). The atmospheric and oceanic components interact once per day exchanging heat, fresh water, and momentum. A fixed annual cycle of heat and freshwater flux adjustment fields computed from a preliminary run of the coupled model are applied over both ice-covered and open ocean, and do not change as the climate evolves. The flux adjustment has been applied in some climate modelling and is used to account for biases in various components that would otherwise cause the model to exhibit a secular drift in its control climate. All experiments are undertaken as perturbations about this control climate. To avoid any artificial feedbacks associated with these flux adjustments, they are applied in exactly the same way in all experiments. In some regions, in particular those where the ocean becomes ice-covered, the flux adjustment fields can be large and could affect ice formation and thus deep water formation.

The reference simulation has a specified CO_2 concentration of 330 ppm, and a contemporary land mask and topography. This experiment is referred to as "REF". The LGM simulation features a decreased CO_2 concentration of 235 ppm, a value chosen to reproduce the greenhouse gas forcing difference between present and LGM conditions (Barnola et al., 1987), and ice sheet topography using the ICE-4G reconstruction of Peltier (1994). The ice sheet volume requires an estimated LGM sea level drop of 120 m (Fairbanks, 1989). This is equivalent to about 3% of the total ocean volume and results in an increased global mean salinity of about 1 psu (Broecker and Peng, 1982). In the LGM simulation, the land mask is

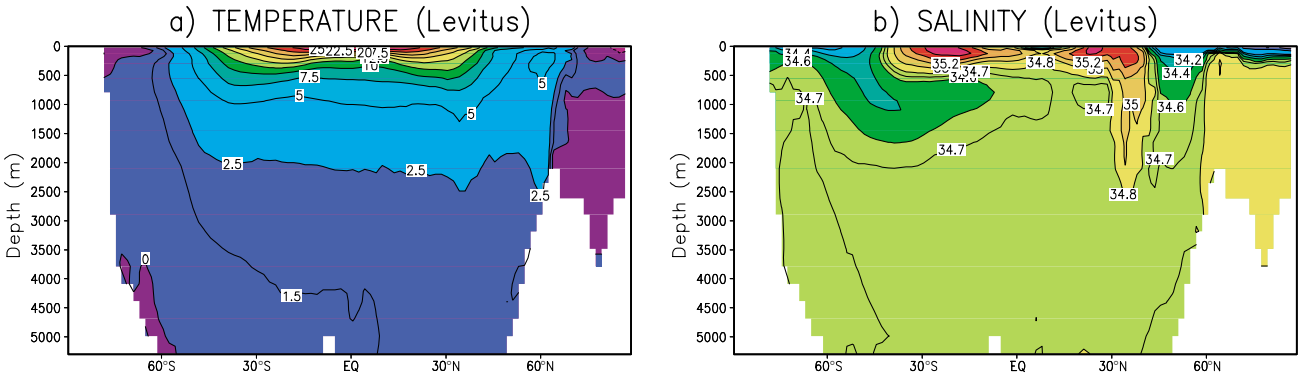

Fig. 1 Zonally averaged annual-mean meridional sections of the observed (a) potential temperature (Levitus and Boyer, 1994) and (b) salinity (Levitus et al., 1994) for the global domain.

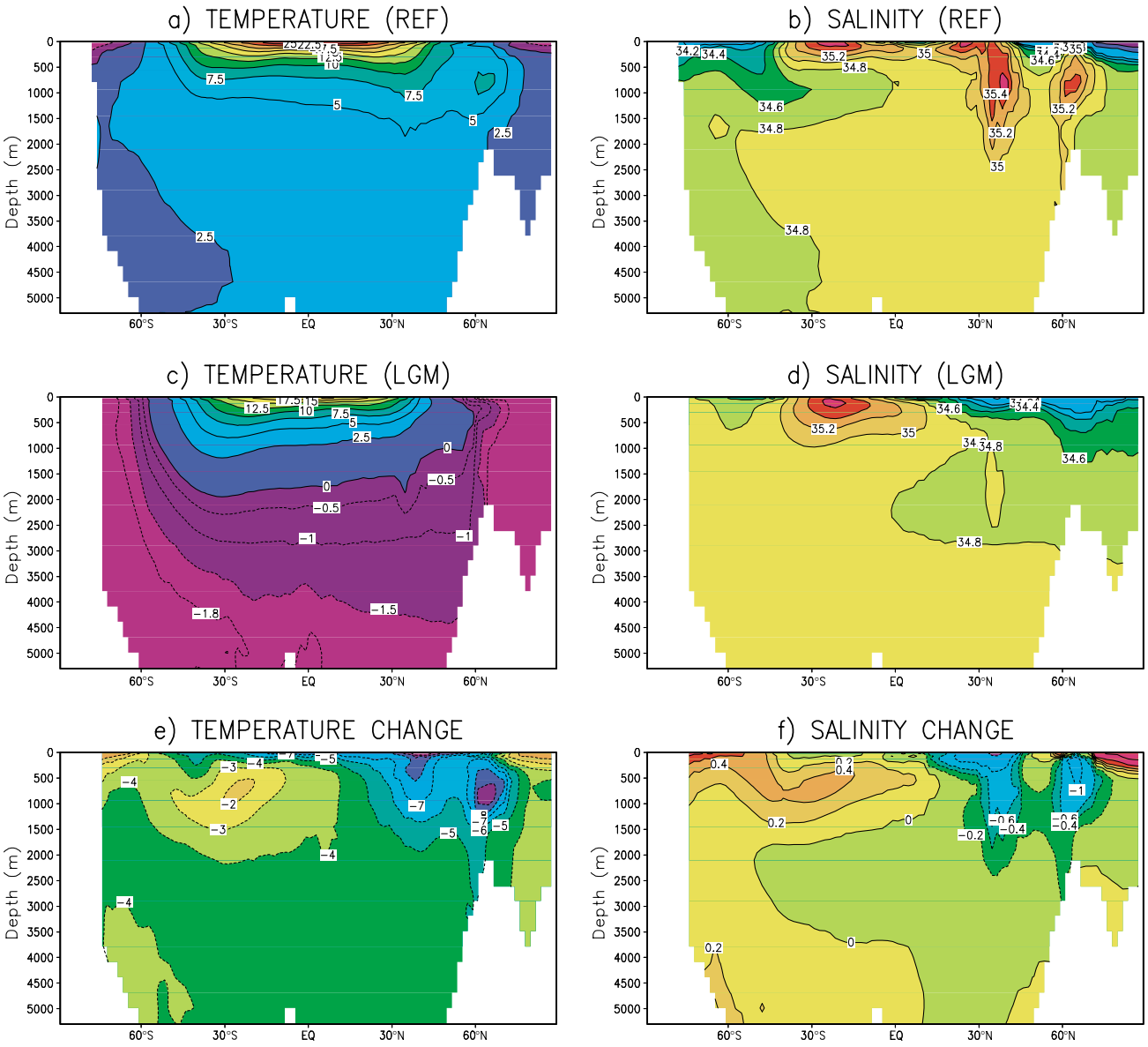

Fig. 2 Zonally averaged annual-mean meridional sections of the simulated (a) potential temperature and (b) salinity for the REF, (c) potential temperature and (d) salinity for the LGM, and (e) potential temperature change and (f) salinity change.

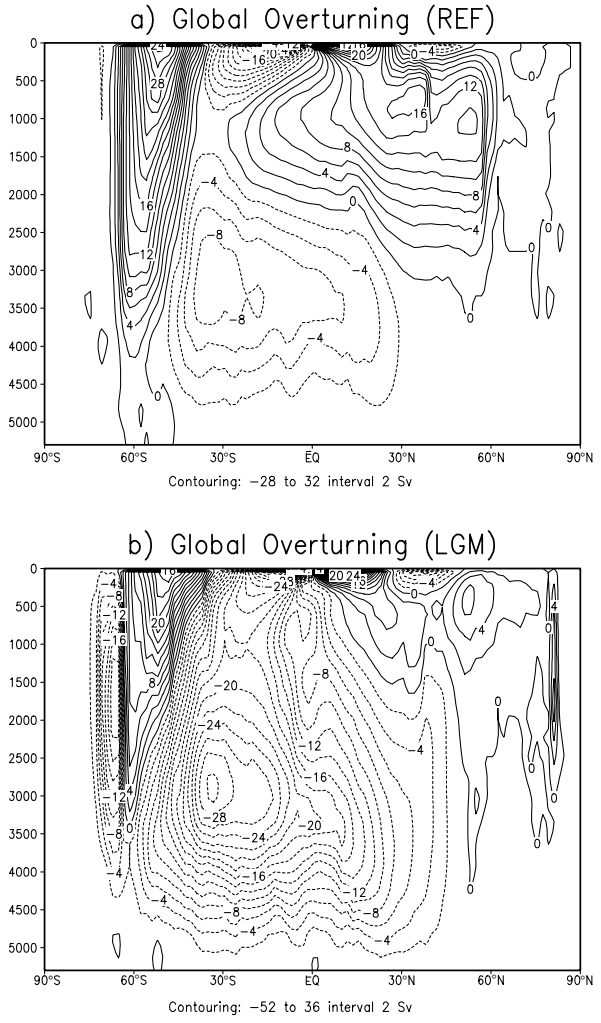

Fig. 3 Annual-mean meridional stream function for the global domain simulated in (a) REF, and (b) LGM. Units are in Sv (10^6 m^3 s^{-1}).

modified to match the sea level change, but the ocean volume (thus the global salinity) is not modified. Orbital parameters and vegetation and soil types are unchanged. This simulation is called "LGM". To save computing effort, the ocean component is accelerated in the LGM simulation using a periodically-synchronous coupling method. A more detailed description of the coupled model and experimental design is found in Kim et al. (2003).

3 Results

Meridional sections of observed potential temperature and salinity in the global domain are shown in Fig. 1 and are presented as a reference for the present-day conditions. These data are from Levitus and Boyer (1994) for the potential temperature and Levitus et al. (1994) for the salinity. The most distinctive feature in the meridional sections is the southward extension of the warm and saline tongue associated with NADW (LCDW in the Southern Ocean). Another salient feature shown in the observed meridional section is the low salinity tongue deepening northward to about 1000 m associated with Antarctic Intermediate Water (AAIW) (Fig. 1b). Lying below CDW, the cold and relatively fresh AABW tongue is also visible.

Figure 2 presents the simulated potential temperature and salinity, zonally averaged in the global domain, for the REF and LGM simulations and their changes. The features found in the observed sections are reproduced reasonably well in the REF simulation. First, the advection of the fresh AAIW tongue to the north is clearly reproduced, although its salinity is slightly higher than that observed. Second, the southward intrusion of the relatively warm and saline NADW tongue is well represented. Third, the relatively cold and fresh AABW tongue is present in the Southern Ocean. Overall, the simulated deep water in the REF simulation is warmer by about 1°C and more saline by about 0.1 psu than the observed values.

The warmer and more saline biases in the REF deep water in comparison to observations seem to be associated with a convection that is too weak in the Southern Ocean and the associated formation of relatively colder and fresher AABW. Figure 3 presents the global meridional overturning stream functions simulated in REF and LGM. In the REF simulation, the simulated overturning circulation associated with the AABW production is about 2 Sv (Fig. 3a), which is weaker than estimates derived from observations (e.g., 8–10 Sv from Orsi et al. (1999)). As a result, the ocean is largely influenced by the relatively warmer and more saline water mass originating in the northern hemisphere in the REF simulation.

With the imposition of glacial boundary conditions, the sea surface temperature decreases and sea surface salinity increases in high latitude oceans, resulting in an increase in surface density with consequent deep convection which exchanges heat between the cold ocean surface and the warmer deep water. This leads to transient anomalous surface warming and an enhancement of turbulent heat fluxes (latent and sensible) (see Kim et al. (2002) for a more detailed analysis). Through this stronger turbulent heat flux, the deep ocean loses heat to the atmosphere and the potential temperature in the deep (below 4000 m) and polar oceans approaches the freezing point in the LGM (Fig. 2c), yielding deep ocean cooling of about 4°C (Fig. 2e). Although this degree of LGM cooling compared to the present day is too large because of a warm bias in the REF deep water, the resultant near-freezing LGM deep ocean temperature in the LGM simulation is supported by the recent palaeoceanographic estimate using sediment core pore fluids and Mg/Ca ratios of benthic fossils (Dwyer et al., 1995; Schrag et al., 1996; Adkins et al., 2002).

The simulated LGM salinity section shows qualitatively different features from that of the present day (Figs 2b and 2d). The high salinity tongue found in the REF northern mid-latitudes, that are associated with the Mediterranean and NADW outflow in the present-day ocean, is absent in the LGM section and the northern hemisphere oceans become fresher overall. The deep ocean freshening in the northern hemisphere originates in the northern North Atlantic where surface salinity is substantially reduced in the LGM simulation

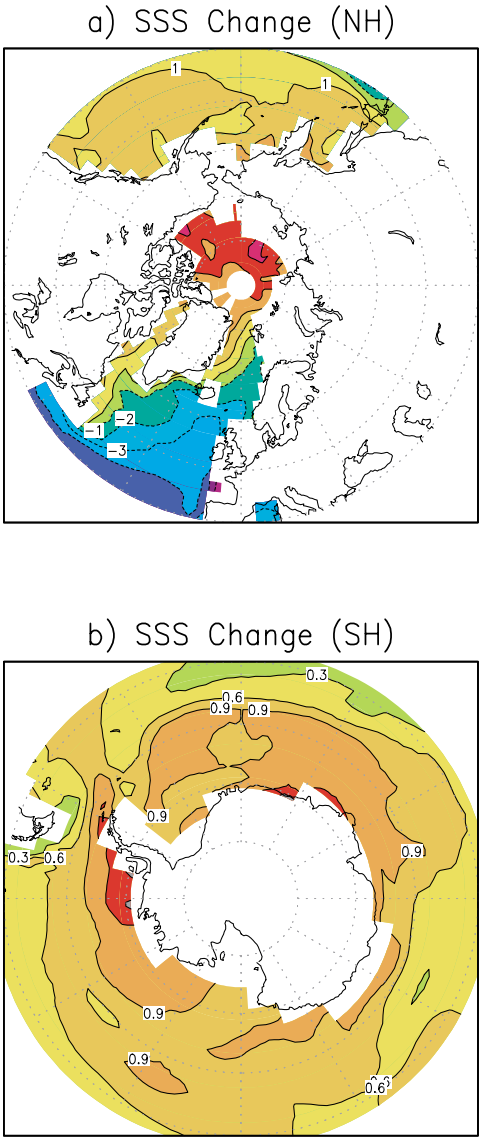

Fig. 4 Geographic distribution of the change in annual-mean sea surface salinity in the (a) northern hemisphere and (b) southern hemisphere.

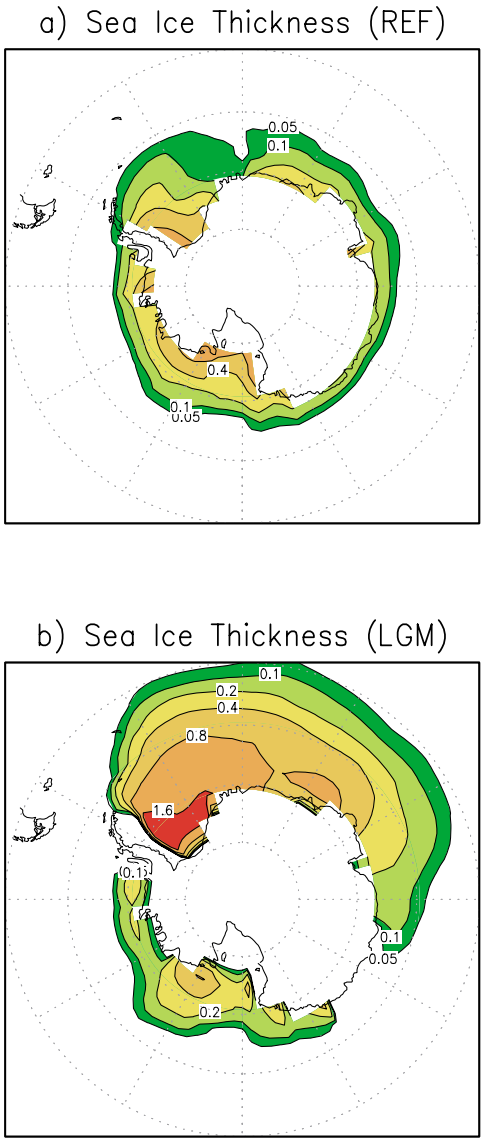

Fig. 5 Geographic distribution of annual-mean sea-ice thickness simulated in (a) REF and (b) LGM. Units are in metres.

(Fig. 4a). As described in Kim et al. (2003), the North Atlantic freshening in the LGM is associated with an increase in local precipitation over evaporation and increased freshwater supply to the North Atlantic from the Mississippi and Amazon rivers. The North Atlantic freshening leads to a substantial weakening of the overturning circulation associated with NADW formation and outflow in the LGM simulation seen in Fig. 3b which is consistent with the palaeoceanographic proxy estimates described in Section 1.

In the Southern Ocean, the deep ocean becomes more saline in the LGM simulation and the AAIW tongue is almost absent (Fig. 2d). The fact that the Southern Ocean deep water is more saline than the northern hemisphere deep ocean in the LGM simulation is consistent with observational proxy estimates by Adkins et al. (2002). They suggest that the Southern Ocean contained the most saline water in the LGM deep ocean. The more saline deep ocean in the southern hemisphere is associated with the change in surface salinity in the Southern Ocean, where salinity increases by more than 0.5 psu in the LGM simulation (Fig. 4b).

The increase in surface salinity in the Southern Ocean is attributed to two primary reasons. First, in the LGM simulation the sea-ice formation and extent increase, especially in the Weddell Sea sector (Fig. 5) and this should increase the release of brine. Adkins et al. (2002) and Schmittner (2003) also attributed the increased salinity in the LGM Southern Ocean to increased sea-ice formation. Second, the coupled model suggests that a drier climate over the southern high latitudes may also have contributed to the higher surface salinity. Figure 6 displays the change in precipitation and the

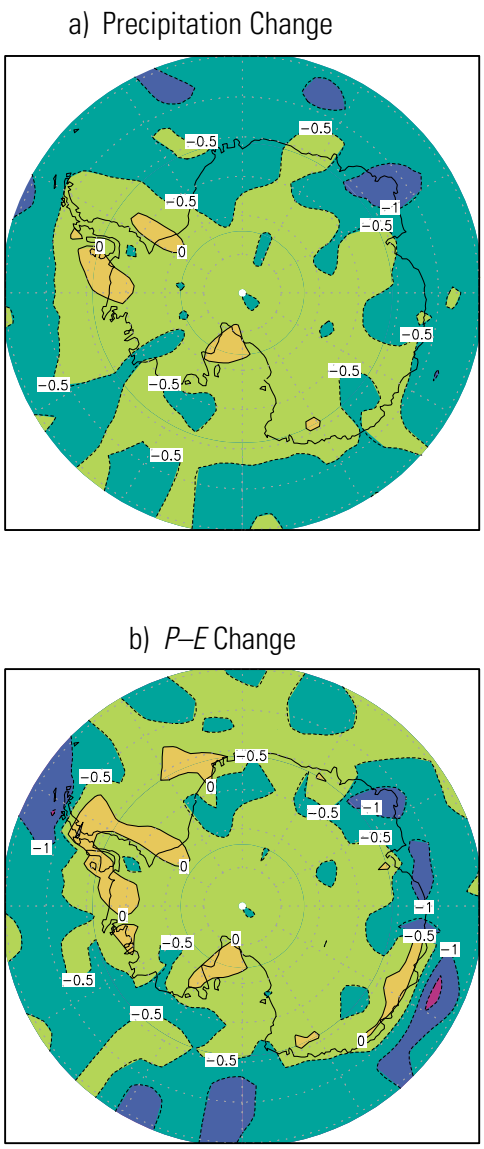

Fig. 6 Geographic distribution of the change in annual-mean (a) precipitation and (b) precipitation (P) minus evaporation (E). Units are in mm d^{-1}.

hydrological budget between the LGM and REF simulations around Antarctica. In the LGM, the precipitation decreases almost everywhere around Antarctica and the change in the precipitation minus evaporation ($P - E$) budget between the LGM and the present day is negative overall, indicating a drier climate. The drier climate over the Southern Ocean, even though the total $P - E$ change is small (less than 0.5 mm d^{-1}, should lead to an additional increase in surface salinity in the LGM. Overall, increased sea-ice formation presumably plays the dominant role in the salinization of AABW as shown by Schmittner (2003).

The colder and more saline surface conditions in the Southern Ocean lead to statically unstable water stratification and active vertical mixing associated with AABW formation and the vigorous overturning circulation associated with AABW outflow (Fig. 3b). The observational proxy estimates of the glacial AABW formation and outflow are not consistent and the uncertainty is large in comparison to that of NADW.

Table 1 summarizes the simulated and observed deep ocean (below 3500 m) temperature and salinity for the present day and the LGM in different ocean basins. The inferred proxy estimates of LGM deep ocean temperature and salinity are based on the results of Schrag et al. (1996) and Adkins et al. (2002) (see Boyle, 2002). As shown in the vertical cross-sections (Fig. 2), the temperature and salinity in the REF simulation are overestimated in comparison to observations although, with regard to the basin, the pattern is consistent. At present, the simulated deep ocean is warmest and most saline in the Atlantic Ocean associated with NADW, while in the LGM the most saline water is found in the Antarctic, consistent with the proxy evidence. The large difference in LGM salinity values between the proxy estimates and the simulation is due to the fact that the LGM simulation does not include the ~1 psu salinity adjustment caused by global ocean volume change. As in the present-day ocean, the coldest water is found in the Southern Ocean in the LGM simulation. This result is in contrast to the proxy estimate which has the Southern Ocean containing the warmest deep water during the LGM.

4 Summary and conclusions

The CCCma coupled model is used to simulate the deep ocean thermohaline properties in the LGM. The imposition of glacial boundary conditions leads to heat loss to the atmosphere from the deep ocean through enhanced vertical mixing and active turbulent heat fluxes. At a near-equilibrium LGM state, the deepwater temperature approaches the freezing point, a result supported by several recent proxy estimates.

The LGM boundary conditions also result in a marked modification of the sea surface salinity. Sea surface salinity decreases in the northern hemisphere, largely due to freshening of the northern North Atlantic, and increases in the Southern Ocean, in part due to an increase in sea-ice formation and a drier climate in the southern high latitudes. The freshening of the northern North Atlantic surface ocean leads to a weakening of vertical convection and the formation and outflow of NADW, whereas in the Southern Ocean the more saline and colder ocean surface leads to the water column becoming statically unstable thus promoting more active vertical mixing and enhancing the formation and outflow of AABW. Eventually, the most saline deep water in the LGM is found in the Southern Ocean, consistent with palaeoceanographic observations.

In conclusion, deep ocean conditions simulated by the coupled model are in reasonable qualitative agreement with observational proxy evidence. The coupled model results largely illustrate the mechanisms responsible for the LGM deep ocean change. In particular, the redistribution of the surface freshwater budget leads to a weaker and shallower North Atlantic overturning circulation and rather different deep ocean thermohaline properties during the LGM.

TABLE 1. The simulated and observed temperature (°C) and salinity (psu) in the deep ocean water (below 3500 m) for the present day and for the LGM. Present day observations are based on Levitus (1994) and the LGM estimate is from Boyle (2002).

	Present Day				LGM			
	Simulated		Observed		Simulated		Inferred	
	T	*S*	*T*	*S*	*T*	*S*	*T*	*S*
Atlantic	3.4	34.97	2.2	34.87	–1.6	34.85	–1.5 ± 0.5	36.0 ± 0.2
Antarctic	1.9	34.72	0.1	34.68	–1.9	34.88	–1.2 ± 0.5	37.2 ± 0.5
Pacific	2.7	34.80	1.5	34.68	–1.3	34.81	–1.3 ± 1.0	36.2 ± 0.1

Acknowledgements

I would like to thank colleagues at the Canadian Centre for Climate modelling and analysis (CCCma), especially Greg Flato and George Boer, for consistent support. Valuable comments from Duke University colleagues, especially Paul Baker, Tom Crowley, Bruce Corliss, Gary Dwyer, and Jesse Kenyon, are appreciated. This study was supported by the Canadian Climate System History and Dynamics (CSHD) program, and through Studies on the Arctic and Antarctic Environmental Monitoring and Characteristics (PP04108, PP04102) projects of the Korea Polar Research Institute, and the Climate Research Program of KORDI (PE87000).

References

ADKINS, J. F.; K. MCINTYRE AND D.P. SCHRAG. 2002. The salinity, temperature, and $\delta^{18}O$ of the glacial deep ocean. *Science*, **298**: 1769–1773.

BARNOLA, J. M.; D. RAYNAUD, Y. S. KOROTKEVICH and C. LORIUS. 1987. Vostok ice core provides 160000-year record of atmospheric CO_2. *Nature*, **329**: 408–418.

BOYLE, E. A. 1990. Quaternary deep water paleoceanography. *Science*, **249**: 863–870.

———. 2002. Oceanic salt switch. *Science*, **298**: 1724–1725.

——— and L. KEIGWIN. 1982. Deep circulation of the North Atlantic over the last 200,000 years: geochemical evidence. *Science,* **218**: 784–787.

——— and ———. 1987. North Atlantic thermohaline circulation during the past 20,000 years linked to high-latitude surface temperature. *Nature,* **330**: 35–40.

BROECKER, W. S. 1997. Thermohaline circulation, the Achilles heel of our climate system: Will man-made CO_2 upset the current balance? *Science*, **278**: 1582–1589.

——— and T.-H. PENG. 1982. Tracers in the sea. Publication of Lamont-Doherty Geological Observatory, Columbia University, New York. 690 pp.

——— and G. H. DENTON. 1989. The role of ocean–atmosphere reorganization in glacial cycles. *Geochim. Cosmochim. Acta*, **53**: 2465–2501.

BUSH, A. B. and S. G. PHILANDER. 1999. The climate of the Last Glacial Maximum: Results from a coupled atmosphere–ocean general circulation model. *J. Geophys. Res.* **24**: 24509–24525.

CURRY, W. B.; J.-C. DUPLESSY, L. D. LABEYRIE AND N. J. SHACKLETON. 1988. Changes in distribution of $\delta^{13}C$ of deepwater ΣCO_2 between the last glaciation and the Holocene. *Paleoceanogr.* **3**: 317–342.

DICKSON, R. R. and J. BROWN. 1994. The production of North Atlantic Deep Water: Sources, rates, and pathways. *J. Geophys. Res.* **99**(**C6**): 12 319–12 341.

DUPLESSY, J.-C.; J. MOYES and C. PUJOL. 1980. Deep water formation in the North Atlantic ocean during the last ice age. *Nature*, **286**: 476–482.

———; N. J. SHACKLETON, R. G. FAIRBANKS, L. LABEYRIE, D. OPPO and N. KALLEL. 1988. Deep water source variations during the last climatic cycle and their impact on the global deepwater circulation. *Paleoceanogr.* **3**: 343–360.

DWYER, G. S.; T. M. CRONIN, P. A. BAKER, M. E. RAYMO, J. S. BUZAS and T. CORREGE. 1995. North Atlantic Deep Water temperature change during the Late Pliocene and Late Quaternary climate cycles. *Science*, **270**: 1347–1351.

FAIRBANKS, R. G. 1989. A 17000-year glacio-eustatic sea level record: Influence of glacial melting rates on the Younger Dryas event and deep-ocean circulation. *Nature*, **342**: 637–642.

FLATO, G. M. and W. D. HIBLER III. 1992. Modelling pack ice as a cavitating fluid. *J. Phys. Oceanogr.* **22**: 626–651.

——— and G. J. BOER. 2001. Warming asymmetry in climate change simulations. *Geophys. Res. Lett.* **28**: 195–198.

FOSTER, T. D. and E. C. CARMACK. 1976. Frontal zone mixing and Antarctic Bottom Water formation in the southern Weddell Sea. *Deep-Sea Res.* **23**: 301–317.

GENT, P. R. and J. C. MCWILLIAMS. 1990. Isopycnal mixing in ocean circulation models. *J. Phys. Ocenaogr.* **20**: 150–155.

GILL, A. E. 1973. Circulation and bottom water production in the Weddell Sea. *Deep-Sea Res.* **20**: 111–140.

HALL, I. R.; N. MCCAVE, N. J. SHACKLETON, G. P. WEEDON and S. E. HARRIS. 2001. Intensified deep Pacific inflow and ventilation in Pleistocene glacial times. *Nature,* **412**: 809–812.

HEWITT, C. D.; A. C. BROCCOLI, J. F. MITCHELL and R. J. STOUFFER. 2001. A coupled model study of the last glacial maximum: Was part of the North Atlantic relatively warm? *Geophys. Res. Lett.* **28**: 1571–1574.

KILLWORTH, P. D. 1983. Deep convection in the world ocean. *Rev. Geophys.* **21**: 1–26.

KIM, S.-J.; G. M. FLATO, G. J. BOER and N. A. MCFARLANE. 2002. A coupled climate model simulation of the Last Glacial Maximum, Part 1: transient multi-decadal response. *Clim. Dyn.* **19**: 515–537.

———; ——— and ———. 2003. A coupled climate model simulation of the Last Glacial Maximum, Part 2: approach to equilibrium. *Clim. Dyn.* **20**: 635–661.

KITOH, A.; S. MURAKAMI and H. KOIDE. 2001. A simulation of the Last Glacial Maximum with a coupled atmosphere–ocean GCM. *Geophys. Res. Lett.* **28**: 2221–2224.

LEVITUS, S. and T. P. BOYER. 1994. World ocean atlas 1994 Vol. 4: temperature. NOAA Atlas NESDIS 4, US Department of Commerce, 117 pp.

———; R. BURGETT and T. P. BOYER. 1994. World ocean atlas 1994 Vol. 3: salinity. NOAA Atlas NESDIS 3, US Department of Commerce, 99 pp.

MCFARLANE, N. A.; G. J. BOER, J.-P. BLANCHET and M. LAZARE. 1992. The Canadian Climate Centre second-generation general circulation model and its equilibrium climate. *J. Clim.* **5**(**10**): 1013–1044.

OPPO, D. W. and M. HOROWITZ. 2000. Glacial deep water geochemistry: South Atlantic benthic foraminiferal Cd/Ca and ^{13}C evidence. *Paleoceanogr.* **15**: 147–160.

ORSI, A. H.; G. C. JOHNSON and J. L. BULLISTER. 1999. Circulation, mixing, and production of Antarctic Bottom Water. *Prog. Oceanogr.* **43**: 55–109.

PACANOWSKI, R. C.; K. DIXON and A. ROSATI. 1993. The GFDL modular ocean model users guide. GFDL Ocean Group Tech Rep 2. Geophysical Fluid Dynamics Laboratory, Princeton, USA, 46 pp.

PELTIER, W. R. 1994. Ice age paleotopography. *Science,* **265**: 195–201.

RINTOUL, S. R. 1998. On the origin and influence of Adelie Land bottom water. In: *Ocean, Ice, and Atmosphere: Interactions at the Antarctic Continental Margin.* S. S. Jacobs and W. R. Weiss (Eds), Antarctic Research Series, Vol. 75, Am. Geophys. Union, pp. 151–171.

RUTBERG, R.L., S.R. HEMMING and S.L. GOLDSTEIN. 2000. Reduced North Atlantic Deep Water flux to the glacial Southern Ocean inferred from neodymium isotope ratios. *Nature,* **405**: 935–938.

SARNTHEIN, M.; K. WINN, S.J.A. JUNG, J.-C. DUPLESSY, L. LABEYRIE, H. ERIENKEUSER and G. GANSSEN. 1994. Changes in east Atlantic deep water circulation over the last 30,000 years: Eight time slice reconstructions. *Paleoceanogr*. **9**: 209–269.

SCHMITTNER, A. 2003. Southern Ocean sea ice and radiocarbon ages of glacial bottom waters. *Earth Planetary Sci. Letts*, **213**: 53–62.

SCHRAG, D. P.; G. HAMPT and D. W. MURRAY. 1996. Pore fluid constraints on the temperature and oxygen isotopic composition of the glacial ocean. *Science,* **272**: 1930–1932.

SEMTNER, A. J. 1976. A model for thermodynamic growth of sea ice in numerical investigations of climate. *J. Phys. Oceanogr.* **6**: 379–389.

SHIN, S.-I.; Z. LIU, B. OTTO-BLIESNER, E. BRADY, J. KUTZBACH and S. HARRISON. 2003. A simulation of the Last Glacial Maximum climate using the NCAR-CCSM. *Clim. Dyn*. **20**: 127–151.

SIEVERS, H. A. and W. D. NOWLIN, JR. 1984. The stratification and water masses at Drake Passage. *J. Geophys. Res.* **89**: 10489–10514.

SLOYAN, B. M. and S. R. RINTOUL. 2001. The Southern Ocean limb of the global deep overturning circulation. *J. Phys. Oceanogr.* **31**: 143–173.

WARREN, B. A. 1981. Deep circulation of the world ocean. In: *Evolution of Physical Oceanography*. B. A. Warren and C. Wunsch (Eds), The MIT Press. pp. 6–41.

WHITWORTH III, T.; A. H. ORSI, S.-J. KIM, W. D. NOWLIN, JR. and R. A. LOCARNINI. 1998. Water masses and mixing near the Antarctic Slope Front. In: *Ocean, Ice, and Atmaosphere: Interactions at the Antarctic Continental Margin*. S. S. Jacobs and W. R. Weiss (Eds), Antarctic Research Series, Vol. 75, Am. Geophys. Union, pp. 151–171.